Translation-rotation decoupling of tracers reflects medium-range crystalline order in two-dimensional colloid glasses

Dong Jae Chun,[*] Younghoon Oh,[*] and Bong June Sung[†]
Department of Chemistry, Sogang University, Seoul 04107, Republic of Korea

(Received 30 August 2021; accepted 17 November 2021; published 30 November 2021)

The dynamic heterogeneity and the translation-rotation decoupling are the dynamic signatures of glasses and supercooled liquids. Whether and how the dynamic heterogeneity would relate to the local structure of glasses has been a puzzle for decades. In this work we perform molecular dynamics simulations for tracers in both two-dimensional polydisperse colloids (2DPC) and two-dimensional binary colloids (2DBC). In 2DPC glasses, hexatic local structures develop at low enough temperatures and grow quickly along with the dynamic correlation length of the 2DPC, which is well known as the medium-range crystalline order (MRCO). In 2DBC glasses, on the other hand, any explicit local structure has not been reported to grow significantly with the dynamic correlation length at low temperatures. We introduce two different types of tracers into colloidal systems: A diamond tracer that resembles the MRCO of 2DPC glasses and a square tracer that is dissimilar to any local structure of glasses. The translation-rotation decoupling of the diamond tracer in 2DPC glasses is much more significant than that of the square tracer in the same 2DPC glasses. On the other hand, such a tracer shape-dependence of the decoupling is not observed in 2DBC glasses where the local hexatic structure does not develop significantly. We introduce a shape-dependency parameter of the decoupling and find that the shape-dependency parameter grows along with the dynamic correlation length in 2DPC glasses but not in 2DBC glasses. This illustrates that the dynamic heterogeneity and the translation-rotation decoupling of tracers could reveal the local structure that develops in glasses.

DOI: 10.1103/PhysRevE.104.054615

I. INTRODUCTION

The dynamics of glass becomes extremely slow and spatially heterogeneous such that even the fluctuation-dissipation theorem, the cornerstone of the statistical mechanics, breaks down [1–7]. Such intriguing dynamic behaviors play critical roles in the kinetics of various systems, including colloidal suspensions, gels, porous materials, plastic crystals [8–10], cell cytoplasms [11–19], and cell membranes [19–22]. Whether the slow and heterogeneous dynamics would relate to any structural order in glasses has been an important question for decades [23–38]. The presence of structural order and the divergence of its correlation length near the glass transition would indicate that the glass transition should be a thermodynamic transition instead of a kinetic phenomenon [28,38–42]. There have been, therefore, tremendous efforts to identify structural orders in various glass-forming liquids [42–49], which turns out to be formidable partly due to the difficulty in obtaining the position vectors of molecules, especially in experiments [49,50]. Instead, tracers, labeled and tracked in single molecule experiments, were often employed to interrogate the dynamics of the glassy matrix [51–57]. In this work we illustrate that one can take an advantage of the breakdown of the fluctuation-dissipation theorem of the tracer dynamics in order to search for the structural order in glasses.

Two-dimensional colloidal liquids should be important systems to study the relation between the inherent structural order and the intriguing dynamics, because one may take a track of colloidal particles readily in both experiments and simulations [31,58–62]. More importantly, depending on the size distribution of particles, the two-dimensional colloidal liquids may or may not develop local structural orders near the glass transition [63–66]. In case of two-dimensional polydisperse colloid (2DPC) glasses, where the size distribution function of particles is Gaussian, the hexatic order develops strongly near the glass transition such that the correlation length (ξ_6) of the hexatic order grows significantly along with the dynamic correlation length (ξ_4) [28,31,43,47,63,67]. On the other hand, for two-dimensional binary colloid (2DBC) glasses, the hexatic order develops relatively weakly such that the hexatic order should not account for the divergence of ξ_4 near the glass transition [28,38,68–70]. Tong and Tanaka proposed a structural order parameter recently which relates to the local packing capability [38,39]. The structural order parameter measures the deviation of the local packing from the optimized configuration where particles are packed most efficiently. The structural order parameter accounts for the slow dynamics of both 2DPC and 2DBC glasses successfully. In this study we compare the local structural orders of 2DPC and 2DBC glasses by taking a track of tracers. We insert two different types of tracers: (1) a diamond tracer that resembles the hexatic structure and (2) a square tracer that is dissimilar to any local structure in two-dimensional (2D) colloidal liquids. We find that the tracer dynamics can reveal the difference between 2DPC and 2DBC glasses clearly.

[*]These authors contributed equally to the work.
[†]Corresponding author: bjsung@sogang.ac.kr

The transport of tracers in glasses and supercooled liquids couples to the structure and the slow dynamics of matrices. This allows one to glean information on the matrices from the tracer transport [71–73]. For example, the diffusion of tracers in gels depends on both the size of tracers and the porosity of the gels. The spatiotemporal correlation of tracers provides information on the local porosity and the local viscosity of the gels [74,75]. The glass transition temperature and the spatially heterogeneous dynamics of thin polymer films have been also investigated by employing small dye molecules as tracers that reflected the segmental dynamics of polymer chains [55]. In this work we insert two different types of tracers (of very low concentrations) in 2D colloidal liquids. We find that the tracer transport of two different types of tracers can provide information on whether the local structure develops near the glass transition or not and how the local structure of the glasses, if any, would grow like a dynamic correlation length.

The fluctuation-dissipation theorem suggests that the translational diffusion coefficient (D_T) and the rotational diffusion coefficient (D_R) should obey the Stokes-Einstein (SE) and the Debye-Stokes-Einstein (DSE) relations, respectively. In other words, both D_T and D_R should be proportional to the ratio of the temperature (T) to the viscosity (η). Therefore the translation and the rotation couple to each other such that the ratio (D_T/D_R) of two diffusion coefficients should stay constant over a range of T. In glasses and supercooled liquids, however, D_T/D_R of tracers is not constant over a wide range of T, which is called the translation-rotation decoupling [1,76–78]. Since SE and DSE relations are rooted in the fluctuation-dissipation theorem, the translation-rotation decoupling indicates that the fluctuation-dissipation theorem breaks down in glasses. How the decoupling occurs in glasses and whether the decoupling would relate to any structural order in glasses should be, therefore, a topic of importance. In this study we find that the translation and the rotation of both diamond and square tracers decouple in 2DPC and 2DBC glasses. More interestingly, the rotation of diamond tracers (which resembles the local hexatic structure of 2DPC glasses) is suppressed significantly only in 2DPC glasses. This makes the trend of the translation-rotation decoupling of tracers dependent on the local structure of glasses. We define a shape-dependency parameter (Ω) of the decoupling and find that Ω grows well along with the divergent dynamic correlation length.

The rest of the paper is organized as follows. In Sec. II we describe the simulation model and methods to analyze the structures and dynamics. In Sec. III we first investigate the structures and dynamics of 2D colloidal liquids over a range of temperature. Then, we choose three sets of comparisons of 2DPC and 2DBC according to their structural changes. The tracer transport is discussed in each comparison set. In Sec. IV, a summary and conclusions are presented.

II. METHODS

A. Model and methods

We perform molecular dynamics simulations for 2DPC and 2DBC liquids. We prepare initial configurations for two-dimensional colloidal liquids by placing disks at random positions with periodic boundary conditions in all directions. If there were to be any overlap between disks, new random configurations are tried. In case of 2DPC liquids, we sample the diameter (σ_i) of the ith disk randomly from Gaussian distribution. The polydispersity (Δ) is defined as $\Delta = \frac{\sqrt{\langle\sigma^2\rangle - \langle\sigma\rangle^2}}{\langle\sigma\rangle}$, where $\langle\sigma^2\rangle - \langle\sigma\rangle^2$ and $\langle\sigma\rangle$ denote the variance and the average of diameters of disks. $\langle\sigma\rangle = 1\sigma$ and σ is the unit of the length in our study. Δ ranges from 0 to 16%. 2DBC liquids consist of two types of disks, of which diameters are $\sigma_S = 1\sigma$ and σ_L, respectively. In our study we fix the number ratio between large and small disks to be 1 while we change the size ratio ($\Lambda \equiv \sigma_L/\sigma_S$) from 1.1 to 1.4. For both 2DPC and 2DBC liquids, the area fraction $\phi = \sum_{i=1}^{N} \pi\sigma_i^2/4L^2 \approx 0.7$ is fixed. Here, the dimension (L) of our simulation system is $L = 64\sigma$. The total number (N) of disks is $N = 3578$ for 2DPC and $N = 2432$–3256 for 2DBC.

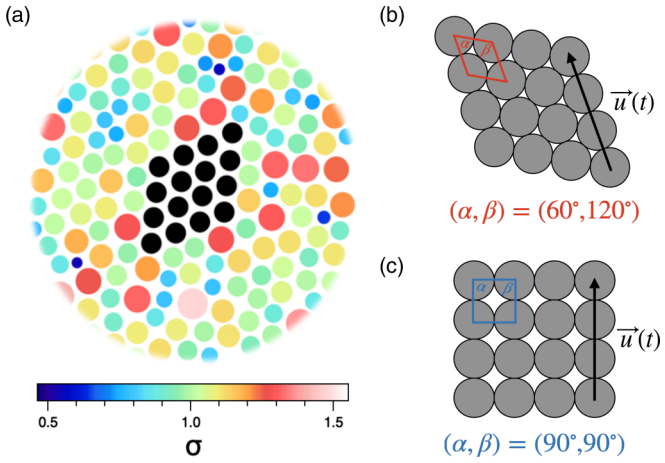

FIG. 1. (a) A representative snapshot of the part of the simulation system of 2DPC of $\Delta = 16\%$ with a diamond tracer at $T = 0.3$. The diamond tracer consists of black disks, while 2D colloidal disks are colored in different colors depending on their diameters (σ_i). The structures of (b) the diamond tracer and (c) the square tracer. The angles (α, β) between two neighbor bond vectors (that share a common disk) are (60°, 120°) and (90°, 90°) for the diamond and the square tracers, respectively. $\vec{u}(t)$ is the unit vector that is parallel to the side of a tracer at time t.

Disks interact with each other via truncated and shifted Lennard-Jones potential (U_{ij}) as follows:

$$U_{ij}(r) = 4\epsilon[(r/\sigma_{ij})^{12} - (r/\sigma_{ij})^{6}] - U_c, \quad r \leqslant r_c, \qquad (1)$$

where $U_c = 4\epsilon[(r_c/\sigma_{ij})^{12} - (r_c/\sigma_{ij})^{6}]$, $r_c = 2.5\sigma_{ij}$, and $\sigma_{ij} = (\sigma_i + \sigma_j)/2$. For $r > r_c$, $U_{ij}(r) = 0$. The mass (m_i) of the ith disk is proportional to the area of the disk, i.e., $m_i \propto \sigma_i^2$. The unit (m) of mass is set as the mass of the disk of $\sigma_i = 1\sigma$. k_BT is also employed as the unit of energy, where k_B is the Boltzmann constant. The unit (τ) of time is, then, $\tau = \sqrt{m\sigma^2/k_BT}$.

We introduce two different types of tracers: diamond and square tracers. Each tracer consists of 16 identical disks of diameter 1σ and mass $1m$ [Figs. 1(b) and 1(c)]. In order to maintain the shape of the tracer throughout simulations, we introduce bonding (U_b) and angle (U_a) potentials with relatively large force constants to the tracers. The harmonic bonding potential U_b is defined as $U_b \equiv 100k_BT(r/\sigma - 1.2)^2$, where r is the distance between a pair of bonded neighbor disks. The harmonic angle potential U_a is also defined similarly as

$U_a \equiv 100 k_b T(\theta - \theta_0)^2$, where θ denotes the angle between two bonds that share a common disk. θ_0 is the value of θ at the minimum of U_a. In case of a diamond tracer, $\theta_0 = \pi/3$ or $2\pi/3$ [Fig. 1(b)]. On the other hand, for a square tracer, $\theta_0 = \pi/2$ [Fig. 1(c)]. The interaction between the disk of tracers and a colloidal disk is described via $U_{ij}(r)$. We insert a single tracer in 2D colloidal liquids at random positions without any overlap between disks [Fig. 1(a)].

We propagate the systems by performing molecular dynamics simulations with LAMMPS (large-scale atomic/molecular massively parallel simulator) software [79]. We employ the velocity-Verlet integrator and Nosé-Hoover thermostat to obtain trajectories under the canonical NVT ensemble. The time step for the integration is 0.005τ. The initial velocities are sampled randomly from the Maxwell-Boltzmann distribution for a given T. We change the temperature (T) of the system from 0.2 to 2. We equilibrate all the systems until both the kinetic and the potential energies converge. We confirm that the presence of a single tracer in each system does not affect the density, the overall transport, and the structure of 2D colloidal liquids.

B. Structures of colloidal disks

In order to compare 2DPC and 2DBC liquids in a fair fashion, we estimate the degree of the disorderedness (ω) that is introduced by Hamanaka and Onuki [64]. Even if the size distributions of 2DPC and 2DBC are different from each other, ω allows us to compare the dynamic properties of both tracers and colloids in 2DPC and 2DBC liquids of comparable disorderedness (ω). First, we calculate the disorderedness (ω_j) for the jth disk by using $\omega_j = \sum_i^{N_j} |\psi_6^j - \psi_6^i|^2$, where $\psi_6^j = (1/N_j)\sum_{k=1}^{N_j} \exp(-i6\theta_{jk})$ and θ_{jk} is the angle between a vector from the jth disk to its kth neighbor disk and an arbitrary reference vector. Here, the ith disk is the neighbor of the jth disk. N_j denotes the number of neighbor disks around the jth disk. If the jth disk and neighbor disks construct a perfect hexagonal structure around the jth disk, $\omega_j = 0$. The overall disorderedness of the system is defined as $\omega \equiv \sum_{j=1}^{N} \omega_j/N$. A larger value of ω indicates that the system is more disordered like liquids.

To investigate the structural transition of the 2D colloidal liquids, we calculate the susceptibility (χ_6) as follows:

$$\chi_6 = L^2\left[\langle \Psi_6^2 \rangle - \langle \Psi_6 \rangle^2\right], \tag{2}$$

which measures the fluctuations in the order parameter [80–82]. Here, $\Psi_6 \equiv |(1/N)\sum_j^N \psi_6^j|$ is the magnitude of the global orientational order parameter. As shown in Fig. 2, the liquid-to-hexatic phase transitions are observed for relatively monodisperse 2D colloidal liquids (2DPC of $\Delta = 5\%$ and 2DBC of $\Lambda = 1.1$). In such relatively monodisperse 2D colloidal liquids, χ_6 diverges at certain temperatures of $T = 0.8$ and 0.9 for 2DPC of $\Delta = 5\%$ and 2DBC of $\Lambda = 1.1$, respectively. On the other hand, we do not observe any liquid-to-hexatic phase transition for 2DPC of $\Delta = 16\%$ and 2DBC of $\Lambda = 1.3$ and 1.4.

C. Dynamics of colloidal disks and tracers

To investigate the dynamics of tracers, we estimate the translational diffusion coefficient D_T by calculating the mean-squared displacement $\langle[\Delta r(t)]^2\rangle = \langle|\vec{r}(t) - \vec{r}(t=0)|^2\rangle$ and employing the Einstein relation $D_T = \lim_{t\to\infty}\langle[\Delta r(t)]^2\rangle/4t$. $\vec{r}(t)$ represents the position vector of the center of mass of a tracer at time t. We calculate the rotational diffusion coefficient D_R using the mean-squared angular displacement $\langle[\Delta\varphi(t)]^2\rangle = \langle|\varphi(t) - \varphi(t=0)|^2\rangle$ and $D_R = \lim_{t\to\infty}\langle[\Delta\varphi(t)]^2\rangle/2t$, where $\varphi(t)$ is the unbounded angle of the orientational vector $\vec{u}(t)$. We define $\vec{u}(t)$ as the unit vector which is parallel to the side of each tracer [Figs. 1(b) and 1(c)]. Here, $\langle\cdots\rangle$ represents an ensemble average, and we obtain 20 independent trajectories for each condition.

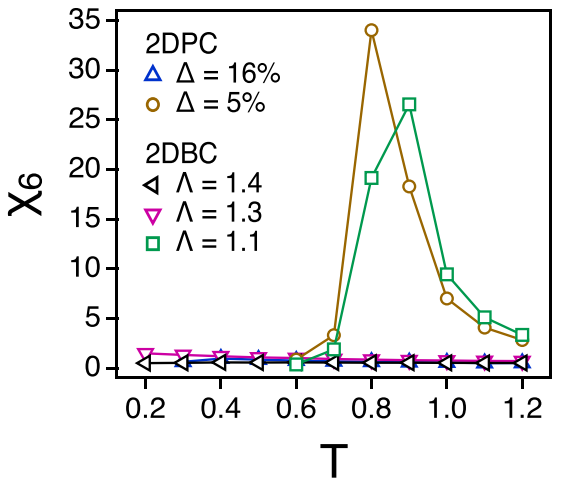

FIG. 2. The susceptibility (χ_6) as a function of T for various 2D colloidal liquids.

We calculate the four-point correlation function in order to investigate dynamics of 2D disks [63,83]. First, a time-dependent order parameter ($Q(t)$) is defined as follows:

$$Q(t) \equiv \sum_i^N \sum_j^N w(|\vec{r}_i(0) - \vec{r}_j(t)|), \tag{3}$$

where $w(r) = 1$ for $r \leqslant 0.3$ or $w(r) = 0$ for $r > 0.3$. $\vec{r}_j(t)$ is the position vector of the jth disk at time t. $Q(t)$ measures the number of disks that overlap between two configurations of the time t and $t = 0$. Then the dynamic susceptibility [$\chi_4(t)$] is obtained by using $\chi_4(t) \equiv (L^2/N^2)[\langle Q(t)^2\rangle - \langle Q(t)\rangle^2]$.

$\chi_4(t)$ could be expressed in terms of four-point density correlation function $g_4(r,t)$, i.e., $\chi_4(t) = \int dr 2\pi r g_4(r,t)$. For a given temperature, $\chi_4(t)$ has a peak at $t = \tau_h$, at which the dynamic heterogeneity is the most significant [Fig. 3(a)]. The first peak position of $\chi_4(t)$ at the lowest temperature is close to the time when the plateau of the self part of intermediate scattering function appears after the fast relaxation (β relaxation).

The pair correlation of overlapping particles, $g_4^{ol}(r,t)$, is defined as

$$g_4^{ol}(r,t) = \frac{1}{N\rho}\left\langle \sum_{ijkl} \delta[\vec{r} - \vec{r}_k(0) + \vec{r}_i(0)] \times w[\vec{r}_i(0) - \vec{r}_j(t)] w[\vec{r}_k(0) - \vec{r}_l(t)] \right\rangle. \tag{4}$$

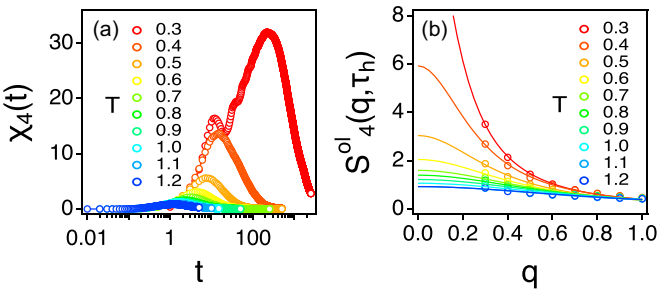

FIG. 3. (a) The dynamic susceptibilities $\chi_4(t)$ in 2DPC of $\Delta = 16\%$. (b) The four-point structure factor (S_4^{ol}) in 2DPC of $\Delta = 16\%$. Symbols are simulation results for S_4^{ol} at various temperatures T and lines are fits to the Ornstein-Zernike equation to estimate the dynamic correlation length ξ_4.

We estimate the dynamic correlation length (ξ_4) by fitting $S_4^{ol}(q,t)$ [the Fourier transform of the self-part of $g_4^{ol}(r, t = \tau_h)$ with $i = j$ and $l = k$] to the Ornstein-Zernike equation with a fitting parameter S_0, i.e.,

$$S_4^{ol}(q,\tau_h) = \frac{S_0}{1+(\xi_4 q)^2}. \quad (5)$$

III. RESULTS AND DISCUSSION

A. Disorderedness and diffusion of 2D colloidal liquids

The structure of 2D colloidal liquids depends on both the size distribution of colloidal disks and the temperature (T). Not surprisingly, as either T decreases or the size distribution becomes narrower, 2D colloids pack more efficiently. As shown in Fig. 4, when the polydispersity (Δ) of 2DPC decreases to 0 or the size ratio (Λ) of 2DBC decreases to 1, the overall disorderedness (ω) of liquids decreases to 0. As T decreases from 2 to 0.2, the colloids pack efficiently and ω decreases (except for 2DBC of large Λ). The glass transition temperatures (T_g) are $T_g \approx 0.2$ and 0.1 for 2DPC of $\Delta = 16\%$ and 2DBC of $\Lambda = 1.4$, respectively. Note that the range of ω of 2DPC liquids is comparable to that of 2DBC liquids in this study.

Depending on T and the size distribution (Δ or Λ), the 2D colloidal liquids stay in different states. In order to discuss the colloidal dynamics for ranges of T and the size distribution,

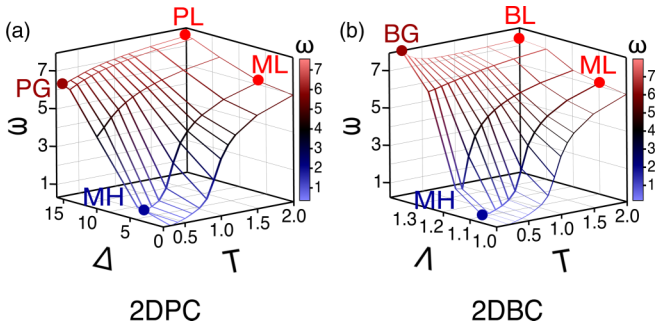

FIG. 4. The overall disorderedness (ω) as a function of T and the size distribution (Δ or Λ) for (a) 2DPC liquids and (b) 2DBC liquids. Δ ranges from 0% to 16% while Λ ranges from 1 to 1.4. The area fraction is fixed at $\phi \approx 0.7$ for 2DPC and 2DBC liquids.

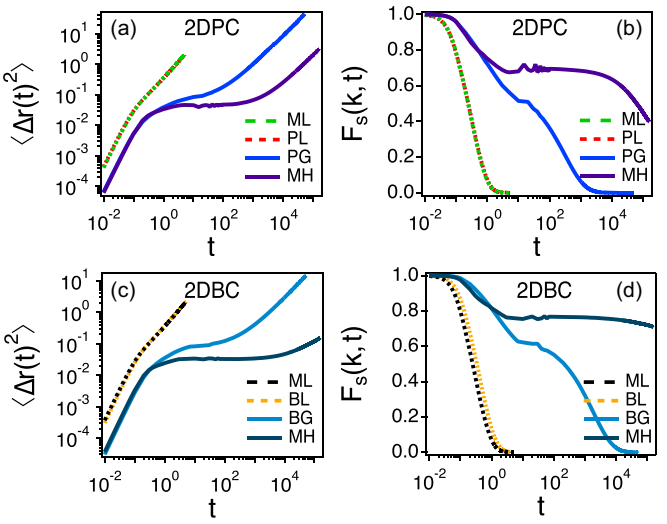

FIG. 5. The mean-square displacements $(\Delta r(t))^2$ and the dynamic structure factors $F_s(k,t)$ of colloidal disks at different limiting cases for 2DPC [(a), (b)] and 2DBC [(c), (d)] liquids. See the text for the description of ML, PL, BL, MH, PG, and BG.

we consider four limiting states for 2DPC liquids: (1) the monodisperse liquid state (ML), (2) the polydisperse liquid state (PL), (3) the monodisperse hexatic state (MH), and (4) the polydisperse glass state (PG). Similarly, in case of 2DBC liquids, we choose four limiting states, too: (1) the ML state, (2) the binary liquid state (BL), (3) the MH state, and (4) the binary glass state (BG). Those limiting state points are marked in Fig. 4.

2D colloidal liquids exhibit very different transport behaviors at four different states as expected. Figure 5 depicts the mean-square displacement $(\Delta r(t))^2$ and the dynamic structure factor $F_s(k,t)$ of colloidal disks at different limiting states. In the MH state of both 2DPC and 2DBC, $(\Delta r(t))^2$ shows a long plateau during more than three orders of magnitude of time t. This indicates that the disks in the MH state hardly diffuse during the intermediate timescales and may diffuse only at long times after the hexagonal structure around the disks may be disturbed by the defects. It has been well known that the defects are inevitable in monodisperse hexatic solid phases and should be the origin for the diffusion of disks at long timescales [84,85]. On the other hand, in the liquid states of ML, PL, and BL states, $(\Delta r(t))^2$ reaches a Fickian regime quickly, i.e., $(\Delta r(t))^2 \sim t^1$, regardless of the size distribution. In case of PG and BG states, $(\Delta r(t))^2$ of both 2DPC and 2DBC systems shows subdiffusive behaviors at relatively short timescales but reaches a Fickian regime at later times in our simulations.

Such characteristic transport behaviors of 2D colloidal liquids in different states are well reflected in $F_s(k,t)$ [Figs. 5(b) and 5(d)]. We employ the value of $2\pi/k$ that corresponds to the first peak of the radial distribution function of colloidal disks $g(r)$. $F_s(k,t)$ decays quickly for liquid states of ML, PL, and BL states. In the case of MH states, $F_s(k,t)$'s do not decay readily in our simulation times. On the other hand, $F_s(k,t)$'s for glass states (PG and BG) do decay within our simulation

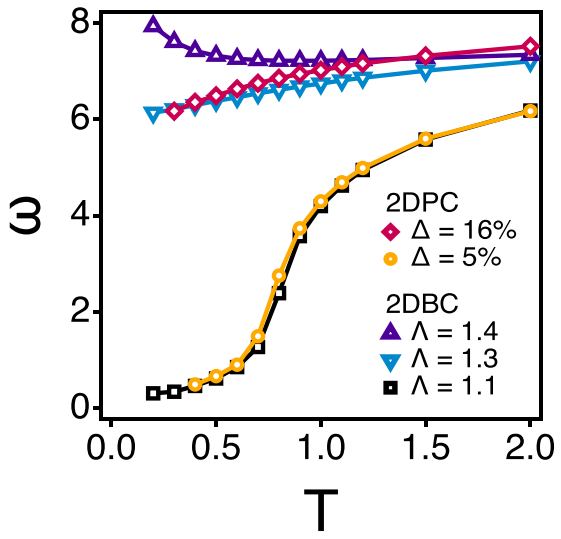

FIG. 6. The overall disorderedness (ω) of 2D colloidal liquids for three sets of comparisons in this study. The set I: 2DPC of $\Delta = 16\%$ and 2DBC of $\Lambda = 1.4$. The set II: 2DPC of $\Delta = 16\%$ and 2DBC of $\Lambda = 1.3$. The set III: 2DPC of $\Delta = 5\%$ and 2DBC of $\Lambda = 1.1$.

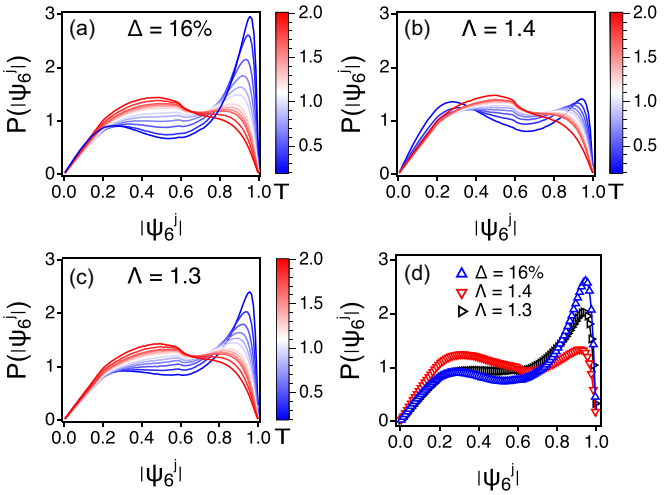

FIG. 7. The probability distribution $P(|\psi_6^j|)$ of the absolute value of ψ_6^j at different temperatures for (a) 2DPC of $\Delta = 16\%$, (b) 2DBC of $\Lambda = 1.4$, and (c) 2DBC of $\Lambda = 1.3$. (d) $P(|\psi_6^j|)$ of those three 2D colloidal liquids at $T = 0.3$.

times but show shoulders at intermediate times, which are the signatures of glassy dynamics.

B. Three sets of comparisons between 2DPC and 2DBC

In this work we consider three sets of comparisons between 2DPC and 2DBC liquids as we decrease T. The values of the overall disorderedness (ω) of 2DPC and 2DBC liquids in each comparison set are close to each other. The first set of comparisons is made between 2DPC of $\Delta = 16\%$ and 2DBC of $\Lambda = 1.4$ (the set I). For those 2D colloidal liquids, $\omega \approx 7$ for both 2DPC and 2DBC liquids at high temperatures around $T = 2$ (Fig. 6). In the set I, ω of 2DPC liquids decreases with a decrease in T such that the hexatic structural order grows. On the other hand, ω of 2DBC liquids (of $\Lambda = 1.4$) increases with a decrease in T, especially at low temperatures. This indicates that 2DBC liquids of $\Lambda = 1.4$ become more disordered at low temperatures.

In the second set of comparisons (set II), we compare 2DPC liquids of $\Delta = 16\%$ with 2DBC liquids of $\Lambda = 1.3$. The disorderedness (ω) of two different types of liquids changes similarly with temperature. ω's for both 2D colloidal liquids decrease from 7 to 6 as T decreases from 2 to 0.2 (Fig. 6). In the third set of comparisons (set III), we compare 2DPC liquids and 2DBC liquids that undergo the liquid-to-hexatic phase transitions. In set III, $\Delta = 5\%$ for 2DPC and $\Lambda = 1.1$ for 2DBC such that those 2D colloidal disks are almost monodisperse. ω's of both colloidal systems decrease quickly to 0 at low temperatures (Fig. 6). Note that at low temperatures, sets I and II correspond to the 2D colloidal glasses while the systems in set III form hexatic solid phases.

Figure 7 depicts the probability distribution ($P(|\psi_6^j|)$) of the absolute value of ψ_6^j for various 2D colloidal liquids at different temperatures. The color code indicates the system temperature. For all 2D colloidal liquids in the figure, the peak of $P(|\psi_6^j|)$ at $|\psi_6^j| \approx 1$ develops as T decreases. In case of 2DBC of $\Lambda = 1.4$ [Fig. 7(b)], however, $P(|\psi_6^j|)$ is relatively insensitive to T compared to 2DPC of $\Delta = 16\%$ and 2DBC of $\Lambda = 1.3$. As expected from the fact that ω's of both 2DPC of $\Delta = 16\%$ and 2DBC of $\Lambda = 1.3$ are similar to each other for all temperature ranges (Fig. 6), $P(|\psi_6^j|)$'s of those two cases are also similar. But the peak of $P(|\psi_6^j|)$ at $|\psi_6^j| \approx 1$ is higher for 2DPC of $\Delta = 16\%$ than for 2DBC of $\Lambda = 1.3$, especially at low temperatures [Fig. 7(d)]. This indicates that at low temperatures, disks in 2DPC of $\Delta = 16\%$ form hexagonal local structures more significantly than 2DBC of $\Lambda = 1.3$.

Even though the overall disorderedness (ω) and $P(|\psi_6^j|)$ of 2DPC of $\Delta = 16\%$ and 2DBC of $\Lambda = 1.3$ (the set II) are similar to each other, the correlation between disks of $|\psi_6^j| \approx 1$ is different. Figures 8(a) and 8(b) depict representative snapshots of 2DPC of $\Delta = 16\%$ and 2DBC of $\Lambda = 1.3$, respectively. The different colors indicate disks of different values of $|\psi_6^j|$. Note that in these snapshots we remove any tracer and perform simulations. In case of 2DPC of $\Delta = 16\%$ [Fig. 8(a)], disks of $|\psi_6^j| \approx 1$ are likely to gather together and

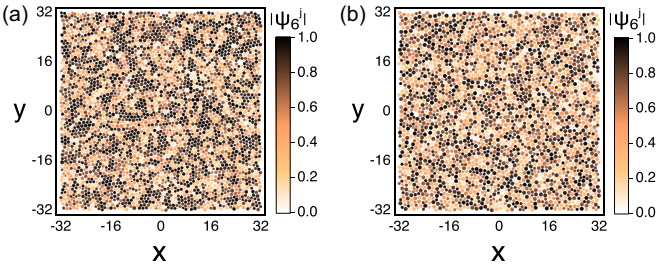

FIG. 8. The representative simulation snapshots at $T = 0.3$ of (a) 2DPC of $\Delta = 16\%$ and (b) 2DBC of $\Lambda = 1.3$. The different colors of disks represent the corresponding values of $|\psi_6^j|$'s. Note that in this set of simulations, we do not introduce any tracer.

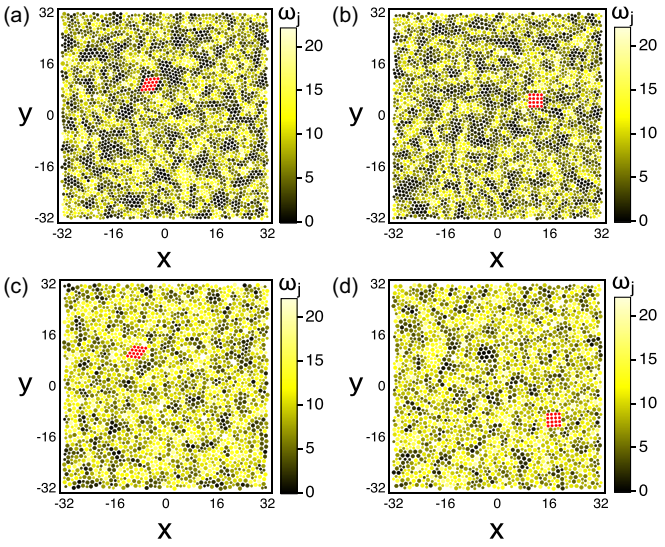

FIG. 9. The representative simulation snapshots at $T = 0.2$ of (a) 2DPC of $\Delta = 16\%$ with a diamond tracer, (b) 2DPC of $\Delta = 16\%$ with a square tracer, (c) 2DBC of $\Lambda = 1.4$ with a diamond tracer, and (d) 2DBC of $\Lambda = 1.4$ with a square tracer. Tracers are colored in red. The different colors of 2D colloidal disks represent their corresponding local disorderedness (ω_j).

form clusters. In case of 2DBC of $\Lambda = 1.3$, however, disks of $|\psi_6^j| \approx 1$ are scattered [Fig. 8(b)].

C. Tracer transport in the comparison set I: 2DPC of $\Delta = 16\%$ vs 2DBC of $\Lambda = 1.4$

We introduce a tracer (either a square or a diamond) into 2DPC of $\Delta = 16\%$ and 2DBC of $\Lambda = 1.4$. Note that the disorderedness (ω) of 2DPC of $\Delta = 16\%$ decreases with a decrease in T, while ω of 2DBC of $\Lambda = 1.4$ increases (Fig. 6). Figure 9 depicts representative simulation snapshots of 2D colloidal liquids with tracers at low temperature. Tracers are colored in red. 2D colloidal disks are colored with different colors depending on the values of ω_j. When a particular disk has a local hexagonal ordering and $\omega_j \approx 0$, the disk is colored in black. On the other hand, when a disk has a disordered local structure, the disk is colored in bright yellow.

As shown in the representative snapshot, a diamond tracer in 2DPC of $\Delta = 16\%$ is surrounded mostly by ordered disks with $\omega_j \approx 0$ [Fig. 9(a)]. On the other hand, a square tracer in 2DPC of $\Delta = 16\%$ is surrounded mostly by yellow disordered disks [Fig. 9(b)]. Because the hexagonal local structure grows significantly in 2DPC of $\Delta = 16\%$ and the diamond tracer is commensurate with the hexagonal local structure, the diamond tracer is more likely to be surrounded by ordered disks, which enhances the packing efficiency and reduces excluded volume and free energy. On the other hand, if a square tracer were to be inserted in the well-ordered hexagonal environment, the square tracer would not be packed efficiently, thus creating a relatively large void around the square tracer inevitably. Therefore the square tracer is more likely to be surrounded by the disordered disks. In case of 2DBC of $\Lambda = 1.4$, on the other hand, the local structures around both diamond and square tracers are not very different from each other [Figs. 9(c) and 9(d)]. This is because a local hexagonal structure does not grow significantly for 2DBC of $\Lambda = 1.4$, and ω increases with a decreasing temperature.

We calculate the probability distribution $P(\omega_j)$ of ω_j of disks around tracers. We decide that a colloidal disk should be a neighbor of the tracer if the distance between the disk and the center of mass of the tracer is smaller than 4σ. Delaunay triangulation may provide a more systematic definition for neighbor particles, because Delaunay triangulation tessellates the system into space for each particle. The choice of the cut-off distance of 4σ seems arbitrary, but our method of choosing a neighbor particle has a merit that the cut-off distance of 4σ works equitably for both polydisperse and binary colloidal systems. When we count the number of neighbor particles around the tracers, the ratios of neighbor disks to the total disks are nearly same at around 0.7% in both polydisperse and binary colloidal systems. This allows us to make a fair comparison between 2DPC and 2DBC. Figures 10(a) and 10(b) depict $P(\omega_j)$'s for different tracers in both 2DPC of $\Delta = 16\%$ and 2DBC of $\Lambda = 1.4$. In 2DBC of $\Lambda = 1.4$, $P(\omega_j)$'s of disks around any type of tracer are very close to $P(\omega_j)$ of all disks in the system (indicated by "Media" in the figure). This indicates that in 2DBC of $\Lambda = 1.4$, tracers of any shape do not prefer any local structure. On the other hand, in 2DPC of $\Delta = 16\%$, $P(\omega_j)$ of disks around a diamond tracer are quite different from that of all disks in the system. Especially, $P(\omega_j)$ of disks around a diamond tracer has quite a large peak at $\omega_j \approx 0$, suggesting that the diamond tracer is surrounded mostly by hexagonally ordered disks as shown in Fig. 9(a). $P(\omega_j)$ of disks around a square tracer is not different from that of all disks.

Such a local structure around a tracer affects the translation-rotation decoupling trend significantly. At high temperatures, the dynamic heterogeneity of systems is not significant such that the translation and the rotation of a tracer couples to each other. Therefore, at $T \approx 1$, the ratio (D_T/D_R) of translational and rotational diffusion coefficients of a tracer stays constant [Figs. 10(d), 10(e), and 10(f)]. As T decreases, the 2D colloidal liquids begin to exhibit glassy dynamics and the dynamic heterogeneity. This leads to the decoupling of the translation and the rotation of a tracer. As shown in Figs. 10(d), 10(e), and 10(f), D_T/D_R increases quickly from 15 to 30 as T decreases. It is interesting that in the case of 2DBC of $\Lambda = 1.4$ where the local hexagonal structure is not dominant, the decoupling trend (i.e., how D_T/D_R increases with a decrease in T) is not sensitive to the tracer shape. In the case of 2DPC of $\Delta = 16\%$ where the local hexagonal structure develops significantly at low temperatures, the translation-rotation decoupling of a diamond tracer is much more significant than that of a square tracer. D_T/D_R increases beyond 30 for a diamond tracer at low temperatures, while D_T/D_R increases up to only about 23 for a square tracer.

Such a dependence of the decoupling trend on the tracer shape in 2DPC of $\Delta = 16\%$ is attributed to the suppressed rotational diffusion of diamond tracers at low temperatures. Figure 10(g) depicts the ratio ($D_{R,\text{square}}/D_{R,\text{diamond}}$ and $D_{T,\text{sqaure}}/D_{T,\text{diamond}}$) of the (both rotational and translational) diffusion coefficient of square tracers to that of diamond tracers as a function of $1/T$. In case of the translational

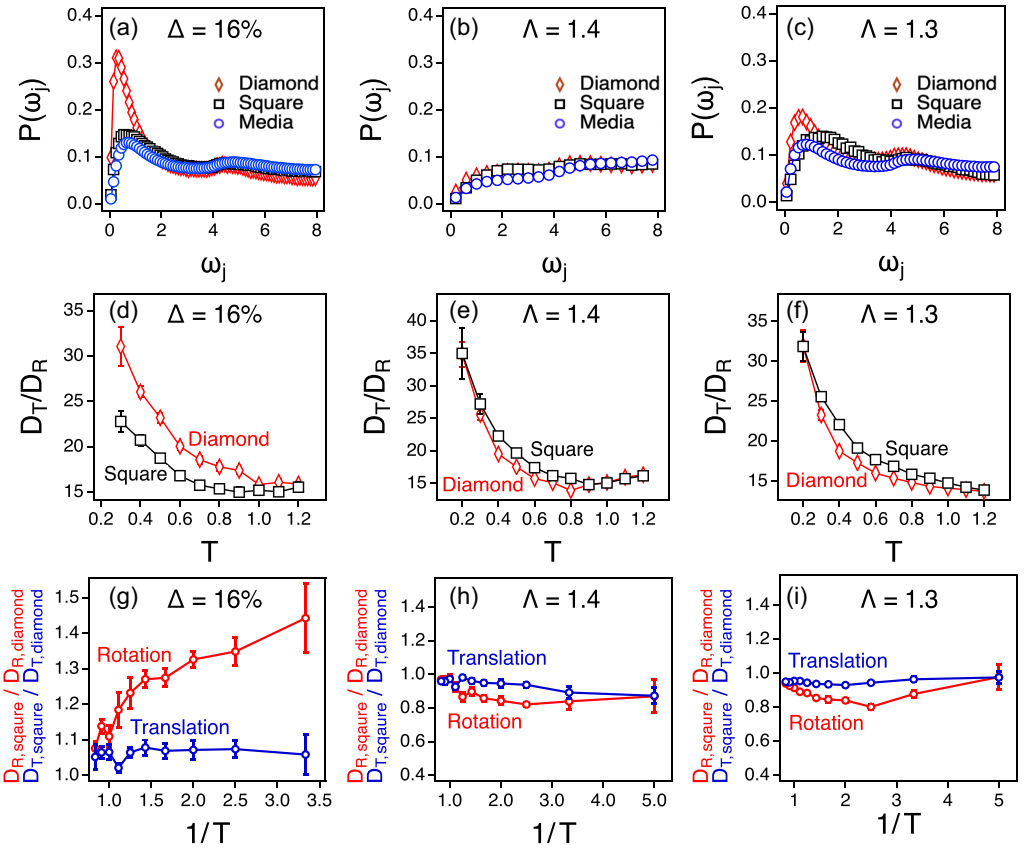

FIG. 10. (a)–(c) The probability distribution functions $P(\omega_j)$ of the local disorderedness ω_j of colloidal disks around tracers at a low temperature for (a) 2DPC of $\Delta = 16\%$ ($T = 0.3$), (b) 2DBC of $\Lambda = 1.4$ ($T = 0.2$), and (c) 2DBC of $\Lambda = 1.3$ ($T = 0.2$). *Media* indicates $P(\omega_j)$ of all colloidal disks without any tracer. (d)–(f) D_T/D_R of tracers as a function of T in (d) 2DPC of $\Delta = 16\%$, (e) 2DBC of $\Lambda = 1.4$, and (f) 2DBC of $\Lambda = 1.3$. (g)–(i) The ratio of (either rotational or translational) diffusion coefficients of the square and the diamond tracers as a function of $1/T$ in (g) 2DPC of $\Delta = 16\%$, (h) 2DBC of $\Lambda = 1.4$, and (i) 2DBC of $\Lambda = 1.3$. Red and blue symbols correspond to the ratios of the rotational and the translational diffusion coefficients, respectively.

diffusion, $D_{T,\text{sqaure}}/D_{T,\text{diamond}}$ stays constant over temperature T. This indicates that the translational diffusion of tracers is relatively insensitive to the tracer shape. On the other hand, $D_{R,square}/D_{R,\text{diamond}}$ increases significantly with a decrease in T (or an increase in $1/T$). This is because the rotational diffusion coefficient ($D_{R,\text{diamond}}$) of a diamond tracer decreases more quickly than $D_{R,square}$ of a square tracer.

The rotational diffusion of a diamond tracer is suppressed more in 2DPC of $\Delta = 16\%$ than that of a square tracer because the diamond tracer is surrounded mostly by hexagonally ordered disks. If the diamond tracer were to rotate, the tracer has to break well-ordered hexagonal structure (made by both the tracer and neighbor disks), which creates a free energy barrier for the diamond rotation. On the other hand, a square tracer is surrounded by disordered disks with a relatively large void such that the free energy barrier for the square rotation should be relatively small. This makes the rotational diffusion in 2DPC of $\Delta = 16\%$ dependent on the tracer shape.

The translational diffusion of tracers is insensitive to the tracer shape even in 2DPC of $\Delta = 16\%$ because we can obtain the translational diffusion constant (D_T) only after tracers diffuse by more than their own size and the tracer diffusion enters a Fickian regime. In other words, D_T can be obtained only after the tracers diffuse over various domains of different mobility and local structure. Therefore D_T is relatively insensitive to the local structure and the tracer shape.

Interestingly, in 2DBC of $\Lambda = 1.4$ where local hexagonal structure is not dominant, both D_T and D_R are insensitive to the tracer shape [Fig. 10(h)]. Both $D_{R,square}/D_{R,\text{diamond}}$ and $D_{T,\text{sqaure}}/D_{T,\text{diamond}}$ stay constant over all the temperature range in this study. This reflects that the local structure of disks around the tracer is not dependent on the tracer shape.

D. Tracer transport in the comparison set II: 2DPC of $\Delta = 16\%$ vs 2DBC of $\Lambda = 1.3$

In this section we compare the transport of tracers in 2DPC of $\Delta = 16\%$ and 2DBC of $\Lambda = 1.3$. Note that the size distribution of 2DBC of $\Lambda = 1.3$ is shallower than that of 2DBC of $\Lambda = 1.4$ in the previous section. Therefore the overall disorderedness (ω) of 2DBC of $\Lambda = 1.3$ is qualitatively different from 2DBC of $\Lambda = 1.4$. At high temperatures of $T \approx 2$, ω's of 2DBC of both $\Lambda = 1.3$ and 1.4 are close to each other at around $\omega \approx 7$. At low temperatures, however, ω of 2DBC of $\Lambda = 1.3$ decreases with a decrease in T while ω of 2DBC of $\Lambda = 1.4$ increases (Fig. 6). Therefore, ω of 2DBC

of $\Lambda = 1.3$ behaves similarly to that of 2DPC of $\Delta = 16\%$, both quantitatively and qualitatively. This indicates that the temperature dependence of the overall disorderedness (ω) of 2D colloidal liquids that we compare in this section is similar. Note, however, that the correlation between disks of large values of $|\psi_6^j|$ is different between 2DBC of $\Lambda = 1.3$ and 2DPC of $\Delta = 16\%$ (Fig. 8).

The response of local 2D disks to the introduction of tracers into 2DPC of $\Delta = 16\%$ is different from that of 2DBC of $\Lambda = 1.3$. Figure 10(c) depicts the distribution functions $P(\omega_j)$ of the local disorderedness (ω_j) of disks that are close to tracers in 2DBC of $\Lambda = 1.3$. Even though the peak of $P(\omega_j)$ at $\omega_j \approx 0$ develops more prominently around a diamond tracer than around a square tracer, $P(\omega_j)$'s of different types of tracers are not very different from each other. On the other hand, in case of 2DPC of $\Delta = 16\%$ as in Fig. 10(a), the peak of $P(\omega_j)$ at $\omega_j \approx 0$ is much higher for the diamond tracer than for the square tracer, such that $P(\omega_j)$ around the diamond tracer is qualitatively different from that around the square tracer. This indicates that the diamond tracer induces the hexagonal local structure in its neighborhood successfully in 2DPC of $\Delta = 16\%$, while the diamond tracer fails to induce the hexagonal local structure in 2DBC of $\Lambda = 1.3$.

Such a difference in the response of the local 2D disks leads to a different behavior of the translation-rotation decoupling. As expected, both diamond and square tracers show the translation-rotation decoupling as T decreases in 2DPC of $\Delta = 16\%$ and 2DBC of $\Lambda = 1.3$ because the 2D colloidal liquids become glassy at low temperatures. In the case of 2DBC of $\Lambda = 1.3$ [Fig. 10(f)], D_T/D_R of the diamond tracer is quite similar to D_T/D_R of the square tracer such that no shape dependency is observed in the decoupling behavior. On the other hand, in 2DPC of $\Delta = 16\%$ [Fig. 10(d)], the translation-rotation decoupling becomes more significant for the diamond tracer than for the square tracer.

Since different tracers in 2DBC of $\Lambda = 1.3$ perturb the local structure to a similar extent [Fig. 10(c)], the temperature dependence of D_T and D_R is similar for different tracers. Figure 10(i) depicts the ratios of diffusion coefficients of tracers ($D_{T,square}/D_{T,\text{diamond}}$ and $D_{R,square}/D_{R,\text{diamond}}$) as functions of $1/T$. Both $D_{T,square}/D_{T,\text{diamond}}$ and $D_{R,square}/D_{R,\text{diamond}}$ stay constant over the temperature range. This is why the translation-rotation decoupling trend is similar for different tracers in 2DBC of $\Lambda = 1.3$. On the other hand, in case of 2DPC of $\Delta = 16\%$, the rotation of a diamond tracer is suppressed more significantly than that of a square tracer as discussed in the previous section. This is attributed to the observation that the diamond tracer induces local hexagonal structure in its neighborhood than the square tracer, which creates a larger free energy barrier for the rotation of the diamond tracer.

Even if the overall disorderedness (ω) is similar in the comparison set II for 2DPC of $\Delta = 16\%$ and 2DBC of $\Lambda = 1.3$, the shape dependency of the translation-rotation decoupling of tracers is very different. This relates to whether a dominant local hexatic structure would grow with a decrease in T or not. When the local hexatic structure grows as in 2DPC of $\Delta = 16\%$, a strong shape-dependency is observed for the translation-rotation decoupling. On the other hand, in case of 2DBC of $\Lambda = 1.3$ where such a local structural order is not observed, the translation-rotation decoupling is not sensitive to the tracer shape.

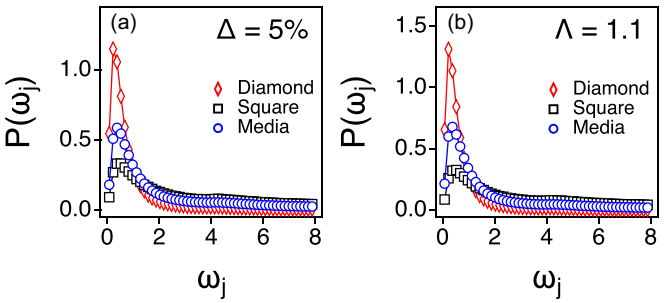

FIG. 11. The probability distribution functions $P(\omega_j)$ of the local disorderedness ω_j of colloidal disks around tracers at $T = 0.8$ for (a) 2DPC of $\Delta = 5\%$ and (b) 2DBC of $\Lambda = 1.1$. *Media* indicates $P(\omega_j)$ of all colloidal disks without any tracer.

E. Tracer transport in the comparison set III: 2DPC of $\Delta = 5\%$ vs 2DBC of $\Lambda = 1.1$

In this section we compare the tracer transport in 2DPC of $\Delta = 5\%$ and 2DBC of $\Lambda = 1.1$. Unlike 2D colloidal liquids in previous sections, both 2DPC of $\Delta = 5\%$ and 2DBC of $\Lambda = 1.1$ are relatively monodisperse such that they undergo the liquid-to-hexatic phase transition at sufficiently low temperatures and the susceptibility χ_6 diverges at the phase transition temperature (Fig. 2). The presence of the liquid-to-hexatic phase transition indicates that the hexatic structure should be a dominant local structure at low temperatures for both 2DPC of $\Delta = 5\%$ and 2DBC of $\Lambda = 1.1$.

When we introduce a diamond tracer (that can be commensurate with the hexatic local structure), the diamond tracer induces the hexatic local structure around the diamond tracer in both 2DPC of $\Delta = 5\%$ and 2DBC of $\Lambda = 1.1$ (Fig. 11). Such a strong induction of the local hexatic structure does not occur for a square tracer. The peak of $P(\omega_j)$ at $\omega_j \approx 0$ develops strongly near the diamond tracer in both 2DPC of $\Delta = 5\%$ and 2DBC of $\Lambda = 1.1$, while the peak does not develop much around the square tracer.

The translation-rotation decoupling is more significant for the diamond tracer in both 2DPC of $\Delta = 5\%$ and 2DBC of $\Lambda = 1.1$ than for the square tracer. Figure 12 depicts the ratio (D_T/D_R) of the translational and rotational diffusion coefficients of tracers. At high temperatures, D_T/D_R stays

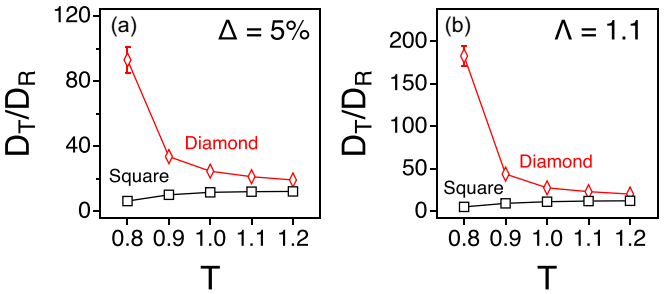

FIG. 12. D_T/D_R of tracers as a function of T in (a) 2DPC of $\Delta = 5\%$ and (b) 2DBC of $\Lambda = 1.1$.

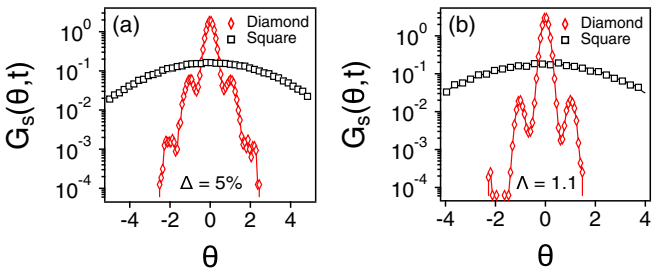

FIG. 13. The self-part of van Hove angular correlation function $[G_s(\theta, t = 4800)]$ of diamond and square tracers at $T = 0.8$ in (a) 2DPC of $\Delta = 5\%$ and (b) 2DBC of $\Lambda = 1.1$.

constant. At the low temperatures, D_T/D_R of the diamond tracer increases up to 100 for 2DPC of $\Delta = 5\%$ and 200 for 2DBC of $\Lambda = 1.1$. We find that such a strong decoupling arises due to the suppressed rotation of the diamond tracer at low temperatures compared to the translation.

At low temperatures in both 2DPC of $\Delta = 5\%$ and 2DBC of $\Lambda = 1.1$, 2D colloidal disks form hexatic phases. Such hexatic structure is commensurate well with a diamond tracer. In order for the diamond tracer to undergo the rotational diffusion, the local hexatic structure should be broken to some extent, which becomes a relatively large free energy barrier for the rotation. In this hexatic phase, the diamond tracer has to undergo rotational hopping motion due to the large free energy barrier. We calculate the self-part of van Hove angular correlation function $G_s(\theta, t) \equiv \langle \delta\{\theta - |\theta(t) - \theta(0)|\}\rangle$ to scrutinize the rotational dynamics of tracers at $T = 0.8$. Here, θ is the unbound rotational angle of the vector $\vec{u}$ of the tracer (Fig. 1). $G_s(\theta, t)$ indicates how much the tracer would rotate during time t. Figure 13 depicts $G_s(\theta, t = 4800)$ of diamond and square tracers in 2DPC of $\Delta = 5\%$ and 2DBC of $\Lambda = 1.1$. $G_s(\theta, t)$'s of the diamond and square tracer are qualitatively different from each other. In case of a diamond tracer, $G_s(\theta, t = 4800)$ has multiple peaks at the multiples of $\theta = \pi/3$, which indicates the rotational hopping motions of the diamond tracer. In the case of a square tracer, on the other hand, $G_s(\theta, t)$ is Gaussian, as expected for the normal rotational diffusion.

F. The shape-dependency parameter of the decoupling

The dynamic correlation length (ξ_4) increases sharply as T decreases toward either the glass transition temperature (for 2DPC of $\Delta = 16\%$, 2DBC of $\Lambda = 1.4$ and 1.3) or the liquid-to-hexatic phase transition temperature (for 2DPC of $\Delta = 5\%$ and 2DBC of $\Lambda = 1.1$), thus indicating the slow and heterogeneous dynamics at low temperatures. Note that according to the previous studies [28,63,68], while ξ_4 increases sharply for both polydisperse and binary 2D colloids, the local hexatic structural order grows along with ξ_4 only for the polydisperse 2D colloidal (2DPC) glasses. The hexatic structural order is not a dominant one for binary 2D colloidal (2DBC) glasses.

As discussed in previous sections, we find that the extent of the translation-rotation decoupling of tracers (which arises due to the dynamic heterogeneity) should be sensitive to the local structural order. Especially when the shape of a tracer is

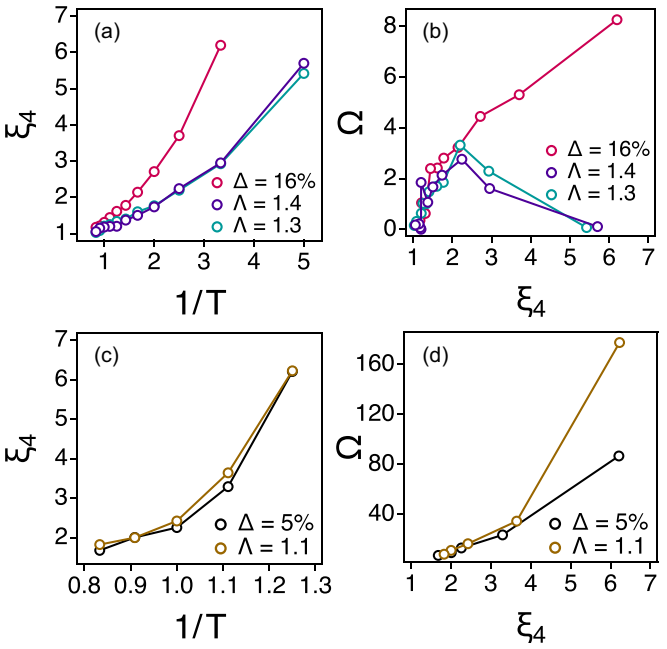

FIG. 14. (a), (c) The dynamic correlation length (ξ_4) of various types of 2D colloidal liquids as a function of $1/T$. (b), (d) The shape-dependency parameter (Ω) of various types of 2D colloidal liquids as a function of ξ_4.

similar to the local structural order of liquids (like a diamond tracer in 2DPC of $\Delta = 16\%$), the rotation of the tracer is suppressed significantly such that D_T/D_R increases sharply as T decreases. On the other hand, when the dominant local structural order does not grow (like in 2DBC of $\Lambda = 1.4$ and 1.3), the decoupling trend is not sensitive to the tracer shape.

In order to quantify such a shape dependency of the decoupling, we define the shape-dependency parameter (Ω) as $\Omega \equiv |(D_T/D_R)_{\text{Diamond}} - (D_T/D_R)_{\text{Square}}|$. Figure 14(b) depicts Ω as a function of ξ_4 for both polydisperse and binary colloidal glasses. In case of 2DPC of $\Delta = 16\%$ where the local hexatic structural order should be a characteristic one, Ω increases along with ξ_4. In the case of 2DBC of $\Lambda = 1.3$ and 1.4 where there is no characteristic local structural order, Ω does not grow with ξ_4. This indicates clearly that the translation-rotation decoupling of tracers reflects the local structural order of glasses. Similarly, for monodisperse 2D colloidal liquids where the liquid-to-hexatic transition occurs at sufficiently low temperatures, Ω increases even more sharply with ξ_4 because the 2D colloids form the hexatic solid phases and the rotation of the diamond tracers is suppressed significantly in the hexatic phases. This suggests that if one were to design and introduce tracers of various shape (which is possible thanks to a modern nanotechnology) into colloidal glasses, one may observe the extent of the translation-rotation decoupling of those tracers and glean information on the local structures of the glasses.

IV. SUMMARY AND CONCLUSIONS

We perform molecular dynamics simulations and investigate the translational and rotational diffusion of a tracer in 2D colloidal systems. 2D colloidal suspensions have been

considered a good testbed to study the structure and the dynamics of glasses and supercooled liquids. We consider two different types of 2D colloids: 2D polydisperse colloids (2DPC) and 2D binary colloids (2DBC). The diameter of each disk in 2DPC liquids is sampled from the Gaussian distribution. The coefficient of variation (Δ) of the disk diameter is employed to represent the polydispersity of 2DPC. On the other hand, 2DBC consists of two types of colloidal disks. The size ratio (Λ) of those two different disks is tuned in this study. Depending on the size distribution (Δ or Λ) and temperature, 2D colloidal systems can be simple liquids, glasses, and hexatic solids. It has been well known that the hexatic structural order grows significantly in the glasses of 2DPC while the hexatic structural order does not grow much in the glasses of 2DBC. We find that the translation-rotation decoupling of a tracer can reflect the presence of such a hexatic structural order in 2D glasses.

We estimate the disorderedness (ω) of both 2DBC and 2DPC. We compare 2DBC and 2DPC with similar values of ω. When we introduce a diamond tracer (that is commensurate with the hexatic local structure) in 2DPC glasses, the diamond tracer induces the hexatic local structure around itself, which creates a free energy barrier for the rotation of the diamond tracer. On the other hand, when we introduce a square tracer (that is dissimilar in any local structure of 2D glasses), the square tracer does not induce the hexatic local structure. Such a different response of 2DPC glasses to the introduction of the different tracers leads to a strong dependence of the translation-rotation decoupling on the tracer shape: The extent of the translation-rotation decoupling is more significant for the diamond tracer than for the square tracer.

In the case of 2DBC glasses where the hexatic structural order does not grow significantly, on the other hand, the translation-rotation decoupling is not dependent on the tracer shape. Both diamond and square tracers do not induce the hexatic local structure much around themselves. We define the shape-dependency parameter (Ω) of the translation-rotation decoupling of tracers. In case of 2DPC glasses where the hexatic structural order grows along with the dynamic correlation length (ξ_4), Ω also correlates with ξ_4 significantly because the translation-rotation decoupling is strongly dependent on the hexatic structural order. In the case of 2DBC glasses where the hexatic structural order is not significant, on the other hand, Ω does not correlate much with ξ_4 because the translation-rotation decoupling is not dependent on the hexatic structural order. This study illustrates that one may interrogate the local structure of glasses, if any, by introducing a tracer of a certain shape and investigating the dynamic heterogeneity and the translation-rotation decoupling of the tracer.

One caveat in our study is that there would be long-wave fluctuations known as Mermin-Wagner fluctuations. Previous studies showed that Mermin-Wagner fluctuations were found in 2D glassy systems and might blur the original glassy dynamics [86–89]. In particular, the transient localization, the signature of glassy dynamics, might be absent in 2D glassy systems. In addition, the translational relaxation and the bond orientational relaxation could be decoupled [88]. And, it should be interesting to investigate the tracer transport in three-dimensional (3D) colloidal systems. The medium-range crystalline order of 3D polydisperse colloids (3DPC) has hcp-like bond orientational order rather than icosahedral order [28,90]. On the other hand, any crystalline structure may not stand for the local structure of 3D binary colloids (3DBC) [38,91]. We may construct hcp-shaped (or icosahedron-shaped) tracers and insert them in both polydisperse and binary colloids. Then we would be able to compare the translation and rotation of those tracers in both 3DPC and 3DBC systems in future studies.

ACKNOWLEDGMENTS

This work was supported by the National Research Foundation of Korea (NRF) grant funded by the Korean government (MSIT) (Grant No. 2019R1A2C2084053).

[1] M. D. Ediger, Spatially heterogeneous dynamics in supercooled liquids, Annu. Rev. Phys. Chem. **51**, 99 (2000).

[2] A. Crisanti and F. Ritort, Violation of the fluctuation–dissipation theorem in glassy systems: Basic notions and the numerical evidence, J. Phys. A: Math. Gen. **36**, R181 (2003).

[3] D. Bonn and W. K. Kegel, Stokes-Einstein relations and the fluctuation-dissipation theorem in a supercooled colloidal fluid, J. Chem. Phys. **118**, 2005 (2003).

[4] T. Kawasaki and H. Tanaka, Apparent Violation of the Fluctuation-Dissipation Theorem Due to Dynamic Heterogeneity in a Model Glass-Forming Liquid, Phys. Rev. Lett. **102**, 185701 (2009).

[5] L. Bellon, S. Ciliberto, and C. Laroche, Violation of the fluctuation-dissipation relation during the formation of a colloidal glass, Europhys. Lett. **53**, 511 (2001).

[6] K. Hayashi and M. Takano, Violation of the fluctuation-dissipation theorem in a protein system, Biophys. J. **93**, 895 (2007).

[7] F. Romá, S. Bustingorry, P. M. Gleiser, and D. Domínguez, Strong Dynamical Heterogeneities in the Violation of the Fluctuation-Dissipation Theorem in Spin Glasses, Phys. Rev. Lett. **98**, 097203 (2007).

[8] R. Brand, P. Lunkenheimer, and A. Loidl, Relaxation dynamics in plastic crystals, J. Chem. Phys. **116**, 10386 (2002).

[9] C. B. Park and B. J. Sung, Heterogeneous rotational dynamics of imidazolium-based organic ionic plastic crystals, J. Phys. Chem. B **124**, 6894 (2020).

[10] H. Park, C. B. Park, and B. J. Sung, The effects of vacancies and their mobility on the dynamic heterogeneity in 1,3-dimethylimidazolium hexafluorophosphate organic ionic plastic crystals, Phys. Chem. Chem. Phys. **23**, 11980 (2021).

[11] M. Sadati, A. Nourhani, J. J. Fredberg, and N. Taheri Qazvini, Glass-like dynamics in the cell and in cellular collectives, WIREs Syst. Biol. Med. **6**, 137 (2014).

[12] B. R. Parry, I. V. Surovtsev, M. T. Cabeen, C. S. O'Hern, E. R. Dufresne, and C. Jacobs-Wagner, The bacterial cytoplasm has

glass-like properties and is fluidized by metabolic activity, Cell **156**, 183 (2014).

[13] A.-S. Coquel, J.-P. Jacob, M. Primet, A. Demarez, M. Dimiccoli, T. Julou, L. Moisan, A. B. Lindner, and H. Berry, Localization of protein aggregation in escherichia coli is governed by diffusion and nucleoid macromolecular crowding effect, PLoS Comput. Biol. **9**, e1003038 (2013).

[14] T. E. Angelini, E. Hannezo, X. Trepat, M. Marquez, J. J. Fredberg, and D. A. Weitz, Glass-like dynamics of collective cell migration, Proc. Natl. Acad. Sci. USA **108**, 4714 (2011).

[15] B. P. English, V. Hauryliuk, A. Sanamrad, S. Tankov, N. H. Dekker, and J. Elf, Single-molecule investigations of the stringent response machinery in living bacterial cells, Proc. Natl. Acad. Sci. USA **108**, E365 (2011).

[16] A. Yethiraj and J. C. Weisshaar, Why are lipid rafts not observed in vivo? Biophys. J. **93**, 3113 (2007).

[17] J. Elf, G.-W. Li, and X. S. Xie, Probing transcription factor dynamics at the single-molecule level in a living cell, Science **316**, 1191 (2007).

[18] J. J. López Cascales, T. F. Otero, B. D. Smith, C. González, and M. Márquez, Model of an asymmetric DPPC/DPPS membrane: Effect of asymmetry on the lipid properties. A molecular dynamics simulation study, J. Phys. Chem. B **110**, 2358 (2006).

[19] D. Bi, J. H. Lopez, J. M. Schwarz, and M. L. Manning, Energy barriers and cell migration in densely packed tissues, Soft Matter **10**, 1885 (2014).

[20] W. He, H. Song, Y. Su, L. Geng, B. J. Ackerson, H. B. Peng, and P. Tong, Dynamic heterogeneity and non-Gaussian statistics for acetylcholine receptors on live cell membrane, Nat. Commun. **7**, 11701 (2016).

[21] Y. Oh, J. Kim, A. Yethiraj, and B. J. Sung, Swing motion as a diffusion mechanism of lipid bilayers in a gel phase, Phys. Rev. E **93**, 012409 (2016).

[22] F. W. Starr, B. Hartmann, and J. F. Douglas, Dynamical clustering and a mechanism for raft-like structures in a model lipid membrane, Soft Matter **10**, 3036 (2014).

[23] X. Yang, R. Liu, M. Yang, W.-H. Wang, and K. Chen, Structures of Local Rearrangements in Soft Colloidal Glasses, Phys. Rev. Lett. **116**, 238003 (2016).

[24] R. L. Jack, A. J. Dunleavy, and C. P. Royall, Information-Theoretic Measurements of Coupling Between Structure and Dynamics in Glass Formers, Phys. Rev. Lett. **113**, 095703 (2014).

[25] A. Malins, J. Eggers, C. P. Royall, S. R. Williams, and H. Tanaka, Identification of long-lived clusters and their link to slow dynamics in a model glass former, J. Chem. Phys. **138**, 12A535 (2013).

[26] M. Leocmach and H. Tanaka, Roles of icosahedral and crystal-like order in the hard spheres glass transition, Nat. Commun. **3**, 974 (2012).

[27] T. Speck, A. Malins, and C. P. Royall, First-Order Phase Transition in a Model Glass Former: Coupling of Local Structure and Dynamics, Phys. Rev. Lett. **109**, 195703 (2012).

[28] H. Tanaka, T. Kawasaki, H. Shintani, and K. Watanabe, Critical-like behaviour of glass-forming liquids, Nat. Mater. **9**, 324 (2010).

[29] C. Patrick Royall, S. R. Williams, T. Ohtsuka, and H. Tanaka, Direct observation of a local structural mechanism for dynamic arrest, Nat. Mater. **7**, 556 (2008).

[30] P. Chaudhuri, S. Karmakar, and C. Dasgupta, Signatures of Dynamical Heterogeneity in the Structure of Glassy Free-Energy Minima, Phys. Rev. Lett. **100**, 125701 (2008).

[31] T. Kawasaki, T. Araki, and H. Tanaka, Correlation Between Dynamic Heterogeneity and Medium-Range Order in Two-Dimensional Glass-Forming Liquids, Phys. Rev. Lett. **99**, 215701 (2007).

[32] G. Biroli, a new kind of phase transition? Nat. Phys. **3**, 222 (2007).

[33] T. S. Jain and J. J. de Pablo, Role of Local Structure on Motions on the Potential Energy Landscape for a Model Supercooled Polymer, J. Chem. Phys. **122**, 174515 (2005).

[34] A. Widmer-Cooper, P. Harrowell, and H. Fynewever, How Reproducible Are Dynamic Heterogeneities in a Supercooled Liquid? Phys. Rev. Lett. **93**, 135701 (2004).

[35] L. Berthier and J. P. Garrahan, Real space origin of temperature crossovers in supercooled liquids, Phys. Rev. E **68**, 041201 (2003).

[36] M. Dzugutov, S. I. Simdyankin, and F. H. M. Zetterling, Decoupling of Diffusion From Structural Relaxation and Spatial Heterogeneity in a Supercooled Simple Liquid, Phys. Rev. Lett. **89**, 195701 (2002).

[37] J. P. Garrahan and D. Chandler, Geometrical Explanation and Scaling of Dynamical Heterogeneities in Glass Forming Systems, Phys. Rev. Lett. **89**, 035704 (2002).

[38] H. Tong and H. Tanaka, Revealing Hidden Structural Order Controlling Both Fast and Slow Glassy Dynamics in Supercooled Liquids, Phys. Rev. X **8**, 011041 (2018).

[39] H. Tong and H. Tanaka, Structural order as a genuine control parameter of dynamics in simple glass formers, Nat. Commun. **10**, 5596 (2019).

[40] C. P. Royall and S. R. Williams, The role of local structure in dynamical arrest, Phys. Rep. **560**, 1 (2015).

[41] C. Cammarota and G. Biroli, Ideal glass transitions by random pinning, Proc. Natl. Acad. Sci. USA **109**, 8850 (2012).

[42] G. Biroli, J.-P. Bouchaud, A. Cavagna, T. S. Grigera, and P. Verrocchio, Thermodynamic signature of growing amorphous order in glass-forming liquids, Nat. Phys. **4**, 771 (2008).

[43] K. Watanabe and H. Tanaka, Direct Observation of Medium-Range Crystalline Order in Granular Liquids Near the Glass Transition, Phys. Rev. Lett. **100**, 158002 (2008).

[44] F. Sausset and G. Tarjus, Growing Static and Dynamic Length Scales in a Glass-Forming Liquid, Phys. Rev. Lett. **104**, 065701 (2010).

[45] M. Mosayebi, E. Del Gado, P. Ilg, and H. C. Öttinger, Probing a Critical Length Scale at the Glass Transition, Phys. Rev. Lett. **104**, 205704 (2010).

[46] G. Biroli, S. Karmakar, and I. Procaccia, Comparison of Static Length Scales Characterizing the Glass Transition, Phys. Rev. Lett. **111**, 165701 (2013).

[47] J. Russo and H. Tanaka, Assessing the role of static length scales behind glassy dynamics in polydisperse hard disks, Proc. Natl. Acad. Sci. USA **112**, 6920 (2015).

[48] J. Kurchan and D. Levine, Order in glassy systems, J. Phys. A: Math. Theor. **44**, 035001 (2010).

[49] F. Sausset and D. Levine, Characterizing Order in Amorphous Systems, Phys. Rev. Lett. **107**, 045501 (2011).

[50] S. Karmakar and G. Parisi, Random pinning glass model, Proc. Natl. Acad. Sci. USA **110**, 2752 (2013).

[51] R. A. L. Vallée, M. Cotlet, J. Hofkens, F. C. De Schryver, and K. Müllen, Spatially heterogeneous dynamics in polymer glasses at room temperature probed by single molecule lifetime fluctuations, Macromolecules **36**, 7752 (2003).

[52] E. Mei, J. Tang, J. M. Vanderkooi, and R. M. Hochstrasser, Motions of single molecules and proteins in trehalose glass, J. Am. Chem. Soc. **125**, 2730 (2003).

[53] J. Jung, T. Kwon, Y. Oh, Y.-R. Lee, and B. J. Sung, Spatial dependence of non-gaussian diffusion of nanoparticles in free-standing thin polymer films, J. Phys. Chem. B **123**, 9250 (2019).

[54] R. A. L. Vallée, W. Paul, and K. Binder, Probe molecules in polymer melts near the glass transition: A molecular dynamics study of chain length effects, J. Chem. Phys. **132**, 034901 (2010).

[55] R. A. L. Vallée, N. Tomczak, L. Kuipers, G. J. Vancso, and N. F. van Hulst, Single Molecule Lifetime Fluctuations Reveal Segmental Dynamics in Polymers, Phys. Rev. Lett. **91**, 038301 (2003).

[56] R. A. L. Vallée, N. Tomczak, G. J. Vancso, L. Kuipers, and N. F. van Hulst, Fluorescence lifetime fluctuations of single molecules probe local density fluctuations in disordered media: A bulk approach, J. Chem. Phys. **122**, 114704 (2005).

[57] K. Paeng, H. Park, D. T. Hoang, and L. J. Kaufman, Ideal probe single-molecule experiments reveal the intrinsic dynamic heterogeneity of a supercooled liquid, Proc. Natl. Acad. Sci. USA **112**, 4952 (2015).

[58] D. N. Perera and P. Harrowell, Stability and structure of a supercooled liquid mixture in two dimensions, Phys. Rev. E **59**, 5721 (1999).

[59] U. Gasser, Crystallization in three- and two-dimensional colloidal suspensions, J. Phys.: Condens. Matter **21**, 203101 (2009).

[60] M. M. Hurley and P. Harrowell, Kinetic structure of a two-dimensional liquid, Phys. Rev. E **52**, 1694 (1995).

[61] G. L. Hunter and E. R. Weeks, The physics of the colloidal glass transition, Rep. Prog. Phys. **75**, 066501 (2012).

[62] B. Li, K. Lou, W. Kob, and S. Granick, Anatomy of cage formation in a two-dimensional glass-forming liquid, Nature (London) **587**, 225 (2020).

[63] T. Kawasaki and H. Tanaka, Structural signature of slow dynamics and dynamic heterogeneity in two-dimensional colloidal liquids: Glassy structural order, J. Phys.: Condens. Matter **23**, 194121 (2011).

[64] T. Hamanaka and A. Onuki, Transitions among crystal, glass, and liquid in a binary mixture with changing particle-size ratio and temperature, Phys. Rev. E **74**, 011506 (2006).

[65] T. Hamanaka and A. Onuki, Heterogeneous dynamics in polycrystal and glass in a binary mixture with changing size dispersity and composition, Phys. Rev. E **75**, 041503 (2007).

[66] E. K. Hobbie, Kinetics of size segregation in quasi-two-dimensional nearly-hard-sphere mixtures, Phys. Rev. E **55**, 6281 (1997).

[67] K. Watanabe, T. Kawasaki, and H. Tanaka, Structural origin of enhanced slow dynamics near a wall in glass-forming systems, Nat. Mater. **10**, 512 (2011).

[68] H. Tanaka, Bond orientational order in liquids: Towards a unified description of water-like anomalies, liquid-liquid transition, glass transition, and crystallization, Eur. Phys. J. E **35**, 113 (2012).

[69] R. M. Ernst, S. R. Nagel, and G. S. Grest, Search for a correlation length in a simulation of the glass transition, Phys. Rev. B **43**, 8070 (1991).

[70] R. D. Mountain and D. Thirumalai, Molecular-dynamics study of glassy and supercooled states of a binary mixture of soft spheres, Phys. Rev. A **36**, 3300 (1987).

[71] H. W. Cho, H. Kim, B. J. Sung, and J. S. Kim, Tracer diffusion in tightly-meshed homogeneous polymer networks: A brownian dynamics simulation study, Polymers **12**, 2067 (2020).

[72] J. Kim and B. J. Sung, Tracer Shape and Local Media Structure Determine the Trend of Translation-Rotation Decoupling in Two-Dimensional Colloids, Phys. Rev. Lett. **115**, 158302 (2015).

[73] Y. Park, J. Kim, and B. J. Sung, Translation-rotation decoupling of tracers of locally favorable structures in glass-forming liquids, J. Chem. Phys. **147**, 124503 (2017).

[74] S. Babu, J. C. Gimel, and T. Nicolai, Tracer diffusion in colloidal gels, J. Phys. Chem. B **112**, 743 (2008).

[75] S. Salami, C. Rondeau-Mouro, J. van Duynhoven, and F. Mariette, Probe mobility in native phosphocaseinate suspensions and in a concentrated rennet gel: effects of probe flexibility and size, J. Agric. Food Chem. **61**, 5870 (2013).

[76] L. Berthier and G. Biroli, Theoretical perspective on the glass transition and amorphous materials, Rev. Mod. Phys. **83**, 587 (2011).

[77] D. Chandler and J. P. Garrahan, Dynamics on the way to forming glass: Bubbles in space-time, Annu. Rev. Phys. Chem. **61**, 191 (2010).

[78] M. T. Cicerone, F. R. Blackburn, and M. D. Ediger, How do molecules move near Tg? Molecular rotation of six probes in o-terphenyl across 14 decades in time, J. Chem. Phys. **102**, 471 (1995).

[79] S. Plimpton, Fast parallel algorithms for short-range molecular dynamics, J. Comput. Phys. **117**, 1 (1995).

[80] K. J. Strandburg, Two-dimensional melting, Rev. Mod. Phys. **60**, 161 (1988).

[81] X. Sun, Y. Li, Y. Ma, and Z. Zhang, Direct observation of melting in a two-dimensional driven granular system, Sci. Rep. **6**, 24056 (2016).

[82] Y. Han, N. Y. Ha, A. M. Alsayed, and A. G. Yodh, Melting of two-dimensional tunable-diameter colloidal crystals, Phys. Rev. E **77**, 041406 (2008).

[83] N. Lačević, F. W. Starr, T. B. Schrøder, and S. C. Glotzer, Spatially heterogeneous dynamics investigated via a time-dependent four-point density correlation function, J. Chem. Phys. **119**, 7372 (2003).

[84] B. van der Meer, W. Qi, J. Sprakel, L. Filion, and M. Dijkstra, Dynamical heterogeneities and defects in two-dimensional soft colloidal crystals, Soft Matter **11**, 9385 (2015).

[85] B. van der Meer, W. Qi, R. G. Fokkink, J. van der Gucht, M. Dijkstra, and J. Sprakel, Highly cooperative stress relaxation in two-dimensional soft colloidal crystals, Proc. Natl. Acad. Sci. USA **111**, 15356 (2014).

[86] S. Vivek, C. P. Kelleher, P. M. Chaikin, and E. R. Weeks, Long-wavelength fluctuations and the glass transition in two dimensions and three dimensions, Proc. Natl. Acad. Sci. USA **114**, 1850 (2017).

[87] B. Illing, S. Fritschi, H. Kaiser, C. L. Klix, G. Maret, and P. Keim, Mermin–Wagner fluctuations in 2D amorphous solids, Proc. Natl. Acad. Sci. USA **114**, 1856 (2017).

[88] E. Flenner and G. Szamel, Fundamental differences between glassy dynamics in two and three dimensions, Nat. Commun. **6**, 7392 (2015).

[89] H. Shiba, Y. Yamada, T. Kawasaki, and K. Kim, Unveiling Dimensionality Dependence of Glassy Dynamics: 2D Infinite Fluctuation Eclipses Inherent Structural Relaxation, Phys. Rev. Lett. **117**, 245701 (2016).

[90] T. Kawasaki and H. Tanaka, Structural origin of dynamic heterogeneity in three-dimensional colloidal glass formers and its link to crystal nucleation, J. Phys.: Condens. Matter **22**, 232102 (2010).

[91] H. Tanaka, H. Tong, R. Shi, and J. Russo, Revealing key structural features hidden in liquids and glasses, Nat. Rev. Phys. **1**, 333 (2019).